


## Degradation of tetracycline by activated peroxodisulfate using a sulfur-modified iron-based material

Shanxue Gao, Nan Zhang and Lei Chen \*

College of Civil Engineering, Nanjing Forestry University, Nanjing 210037, China

\*Corresponding author. E-mail: chenlei\_njfu@163.com

 LC, 0000-0001-7974-1677

### ABSTRACT

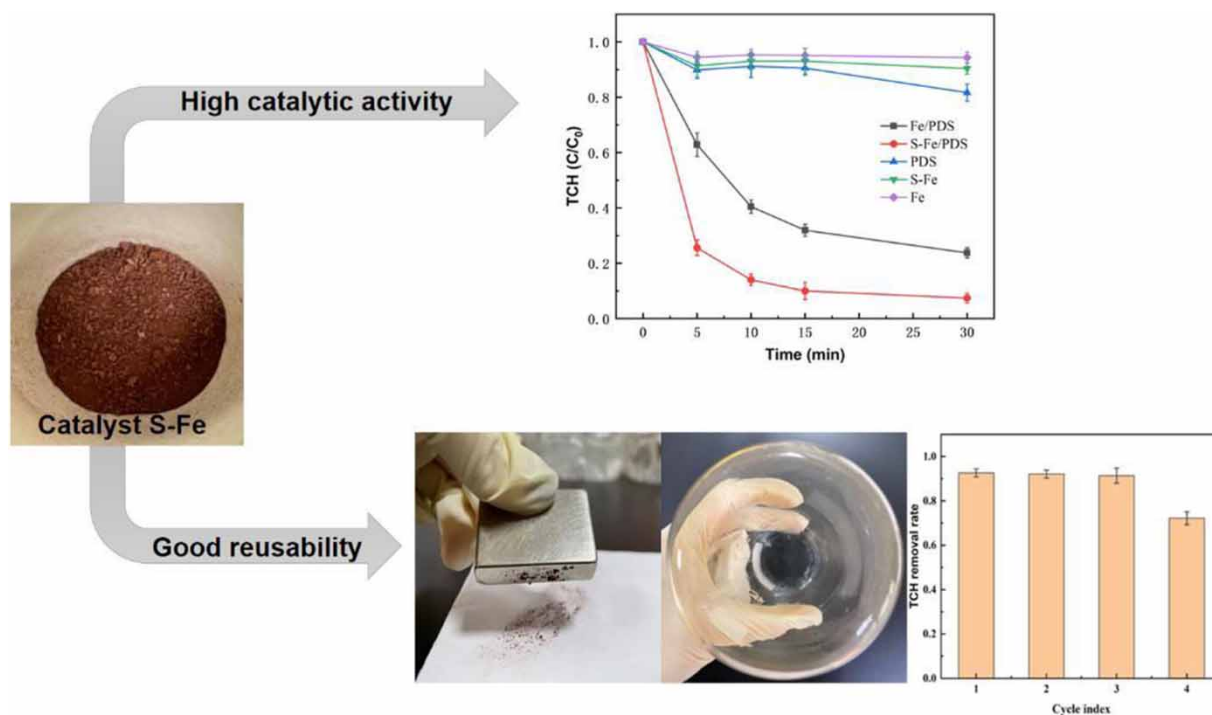
The activation of persulfate by an iron-based catalyst presents a promising approach for the degradation of antibiotics; however, the activation efficiency remains a challenge. Herein, a sulfur-modified iron-based catalyst (S-Fe) by co-precipitation of sodium thiosulfate and ferrous sulfate in a molar ratio of 1:2 was prepared and the efficacy of the S-Fe/PDS system for the removal of tetracycline (TCH) was studied, where a higher removal efficiency was observed compared to the Fe/PDS system. Moreover, the effects of TCH concentration, PDS concentration, initial pH, and catalyst dosage on TCH removal were evaluated, and the highest efficiency was about 92.6% within a 30 min reaction time using a catalyst dosage of 1.0 g/L, a PDS dosage of 2.0 g/L, and a solution pH value of 7. The products and degradation pathways of TCH were analyzed by LC-MS. The free-radical-quenching experiments revealed that both  $\text{SO}_4^{\bullet-}$  and  $\bullet\text{OH}$  radicals contributed to the degradation of TCH in the S-Fe/PDS system, with the former playing a more significant role. The S-Fe catalyst also showed good stability and reusability for the removal of organic pollutants. Our findings suggest that the modification of an iron-based catalyst offers an effective approach to activate persulfate for removal of tetracycline antibiotics.

**Key words:** free radical, iron-based material, peroxodisulfate, tetracycline

### HIGHLIGHTS

- The sulfur-modified iron-based catalyst (S-Fe) was prepared.
- Both  $\text{SO}_4^{\bullet-}$  and  $\bullet\text{OH}$  radicals played the role in the degradation of TCH in the S-Fe/PDS system.
- The S-Fe catalyst showed high catalytic activity and reusability for the removal of organic pollutants.

## GRAPHICAL ABSTRACT



## 1. INTRODUCTION

Microorganisms produce antibiotics through metabolic activities that have been comprehensively utilized to treat various biological diseases (Shen *et al.* 2020). Among the numerous antibiotics used in industrial production and daily use, tetracycline comprises a significant proportion (Nasseri *et al.* 2017). However, the prevalence of tetracycline antibiotics in the environment is concerning, as they may enter water and soil environments via drug abuse and incomplete organism absorption, leading to environmental contamination (Weidner *et al.* 2021). Thus, the development of simple and effective treatment technologies for the removal of tetracycline antibiotics is a pressing priority.

Conventional techniques employed by sewage treatment plants primarily target the elimination of nitrogen, phosphorus, and total organic carbon present in wastewater, but not antibiotics (Kovalakova *et al.* 2020). Numerous approaches have been employed for the removal of tetracycline, including coagulation sedimentation, adsorption (Acosta *et al.* 2016), membrane separation (Li *et al.* 2004), biological treatment (Abejon *et al.* 2015), ozone oxidation (Iakovides *et al.* 2019), electrochemical oxidation (Borisova *et al.* 2013), photocatalytic oxidation (Saadati *et al.* 2016), and Fenton oxidation (Ma *et al.* 2005). Among these, advanced oxidation technology based on persulfate (PS) has garnered significant attention due to its high efficiency, ease of operation, and low cost. By breaking the O–O bond, peroxymonosulfate (PMS) or peroxydisulfate (PDS) generates sulfate radical ( $\text{SO}_4^{\cdot-}$ ) and hydroxyl radical ( $\cdot\text{OH}$ ), augmenting its oxidative degradation capabilities toward organic constituents. Compared with traditional PDS activation methods such as UV- (Waclawek *et al.* 2017), thermal- (Zhang *et al.* 2019), alkali- (Qi *et al.* 2016), activated carbon- (Forouzesheh *et al.* 2019), and transition-metal activation (Zhang *et al.* 2015), sulfur-modified iron-based materials have been proved to significantly increase the catalytic activity of PDS and PMS activation, and avoid secondary pollution (Ling *et al.* 2022). The enhancement of catalyst reactivity through sulfur modification could be attributed to the promotion of  $\text{Fe}^{3+}$  reduction to  $\text{Fe}^{2+}$  and the acceleration of electron transfer between the oxidant and catalyst (Wang *et al.* 2020). Notwithstanding the favorable catalytic properties of sulfur-modified iron-based materials, there remains a need for further improvements in the stability and magnetic properties to enhance their practical applications (Zheng *et al.* 2019). Therefore, it is worth developing a sulfur-modified iron-based catalyst with good reusability and stability as well as high efficiency in activating PDS for removal of organic pollutants.

In this study, the sulfur-modified iron-based catalyst (S-Fe) was prepared through co-precipitation of ferrous sulfate ( $\text{FeSO}_4$ ) and sodium thiosulfate ( $\text{Na}_2\text{S}_2\text{O}_3$ ). The degradation of tetracycline via activated peroxodisulfate, utilizing the S-Fe catalyst, while also the effects of catalyst dosage, pH, and inorganic anions were investigated. Additionally, the involved activation mechanism was studied via quenching experiments. The results will propose a potential alternative method for effective removal of antibiotics from wastewater.

## 2. MATERIAL AND METHODS

### 2.1. Reagents and chemicals

Tetracycline hydrochloride (TCH, purity 96%) was obtained from Aladdin Biochemical Technology Co. (Shanghai, China).  $\text{Na}_2\text{S}_2\text{O}_3$  (AR),  $\text{FeSO}_4$  (AR), tert butanol (TBA, AR), sodium persulfate ( $\text{Na}_2\text{S}_2\text{O}_8$ , AR), sulfuric acid ( $\text{H}_2\text{SO}_4$ , AR), sodium chloride (NaCl, AR), sodium sulfate ( $\text{Na}_2\text{SO}_4$ , AR), and sodium carbonate ( $\text{Na}_2\text{CO}_3$ , AR) were obtained from Sinopharm Group Chemical Reagent Co. (Shanghai, China). Sodium hydroxide (NaOH, AR), sodium nitrate ( $\text{NaNO}_3$ , AR), and methanol (MeOH, AR) were obtained from Nanjing Chemical Reagent Co. (Nanjing, China). The solutions used in this study were prepared with ultrapure water.

### 2.2. Catalyst preparation

$\text{Na}_2\text{S}_2\text{O}_3$  and  $\text{FeSO}_4$  according to the molar ratio of sulfur to iron of 1:2 were dissolved with 100 mL of ultrapure water, as the most optimal yield was achieved at a ratio of approximately 1:2 according to our previous study. Meanwhile, several drops of 10% dilute  $\text{H}_2\text{SO}_4$  were added during the dissolution process to prevent oxidation of ferrous ions ( $\text{Fe}^{2+}$ ). A magnetic stirrer was utilized to stir the mixture for 30 min, and subsequently, NaOH (1 mol/L) was added to adjust the pH to approximately 7. The resulting solution was subjected to filtration through a vacuum suction filtration device, and the filter residue was repeatedly washed with ultrapure water until clear liquid was obtained. The residue was air-dried at 70 °C, then calcined for 1 h in a muffle furnace at 400 °C before it was ground into a powder. The resulting catalyst was labeled as S-Fe. The  $\text{pH}_{\text{zpc}}$  of S-Fe was about 7.2. For the test of reusability, the catalyst was collected and cleaned with water using a vacuum suction filtration method.

### 2.3. Characterization

Scanning electron microscopy (SEM) using a ZEISS Sigma 300 (Zeiss, German) was employed to scrutinize the shape structure, pore size, and surface morphology of S-Fe catalyst. The crystal structures of the samples were analyzed by X-ray diffractometry (XRD) with a Rigaku Ultima IV (Japan), using the  $\text{Cu-K}\alpha$  diffracted ray source at  $2^\theta$ . Furthermore, the element composition of the material surface and the valence distribution of the target element were investigated by using X-ray photoelectron spectroscopy (XPS) with an AXIS UltraDLD (Kratos, UK), employing  $\text{Al-K}\alpha$  as the excitation source. The working current and voltage for the experiment were 16 mA and 12.5 KV, respectively.

### 2.4. Catalytic degradation experiments

All batch experiments were conducted using 250 mL conical flasks that were placed in a shaker and kept at a constant temperature of 25 °C and an agitation rate of 160 rpm. TCH,  $\text{Na}_2\text{S}_2\text{O}_8$ , and S-Fe were added to the conical flasks as the reactants. The effects of TCH initial concentration, PDS concentration, catalyst dosage, and pH on the degradation of TCH by the S-Fe/PDS system were evaluated (Zheng *et al.* 2019; Ling *et al.* 2022). The TCH concentration was set to 20 mg/L, the dosage of S-Fe at 1.0 g/L, the PDS concentration at 2.0 g/L, and the initial pH at 7 during the radical quenching experiment. MeOH or TBA at a volume of 10 mL was also introduced into the reaction system. At predetermined time intervals, 1 mL of the sample was collected and immediately mixed with 1.0 mL of a methanol solution to quench reactive radicals. Afterwards, the samples were immediately filtered through 0.22  $\mu\text{m}$  syringe filters to remove solid impurities. The concentration of residual TCH in the solution was determined by an ultraviolet visible spectrophotometer at a wavelength of 358 nm. The intermediate degradation products of TCH were determined by liquid chromatography-tandem mass spectrometry (Thermo, USA) with a C18 water column (4.6 mm  $\times$  150 mm, 5  $\mu\text{m}$ ) and a DAD detector at 357 nm. The mobile phase was composed of acetonitrile and 0.1% formic acid with a volume ratio of 10–90%. The column temperature was 25 °C, the flow rate was 0.5 mL/min, and the injection volume was 10  $\mu\text{L}$  all at once. An electrospray ion source (EIS) was used with a capillary voltage of 3.5 kV, a capillary temperature of 25 °C, a fragment voltage of 50 kV, a desolvation flow rate of 10 L/min, and a scan range of 50–800  $m/z$ .

### 3. RESULTS AND DISCUSSION

#### 3.1. Characterization

The morphology and particle size of the S-Fe catalyst were examined using SEM at magnifications of 10, 50, and 80k. The surface of S-Fe exhibited a columnar porous structure with a substantial specific surface area. The S-Fe particles ranged in size from 100 to 1,000 nm and formed clusters in the shape of columns or blocks, as illustrated in Figure 1.

The XRD patterns of the S-Fe catalyst are presented in Supplementary Figure S1, revealing evident diffraction peaks at  $2^\theta$  values of  $17.72^\circ$ ,  $24.3^\circ$ ,  $33.02^\circ$ ,  $35.68^\circ$ , and  $53.98^\circ$ . By comparing these peaks with those of iron-based substances on  $\alpha$ -FeO/S (JCPDS-33-0664) standard reference cards, it can be inferred that the peak at  $17.72^\circ$  corresponds to  $\text{Fe}_{12}\text{S}_{11}\text{O}_{51}$ ,  $24.3^\circ$  corresponds to  $\text{FeO}(\text{OH})$ ,  $33.02^\circ$  corresponds to  $\text{FeS}_2$ ,  $35.68^\circ$  corresponds to  $\text{Fe}_3\text{O}_4$ , and  $53.98^\circ$  corresponds to  $\text{FeS}$ , indicating that sulfur was superbly loaded on the surface of the material.

XPS analysis was conducted to investigate the surface element composition and chemical properties of the modified material, and the results are presented in Figure 2(a). Specifically, the XPS spectrum of the S-Fe material indicates characteristic peaks of oxygen (O1s), carbon (C1s), iron (Fe2p), and sulfur (S2p), with respective atomic ratios of 62.04, 26.81, 2.15, and 2.6. However, a certain degree of loss in the element composition of S-Fe was observed when compared with the amount of raw materials added during the process of catalyst preparation, which might result from grinding, heating or wetting. Subsequently, the Fe2p and O1s peak values were processed using Avantage, and the results are shown in Figure 2(b) and 2(c), respectively. The electron layer double peaks of Fe2p at 711.9 and 724.6 eV correspond to the  $2p^{1/2}$  and  $2p^{3/2}$  orbitals of Fe in the narrow spectrum of Fe2p. Notably, the middle of the two Fe2p peaks suggests the presence of zero valent iron in the prepared S-Fe, with a weak peak possibly indicating  $\text{FeS}_2$  at 709.9 eV, consistent with the  $\text{FeS}_2$  diffraction peak in XRD results. The O1s spectra, as shown in Figure 2(c), exhibit peaks at 529.3 and 531.9 eV, corresponding to  $\text{O}^{2-}$  and  $\text{OH}^-$ , respectively.

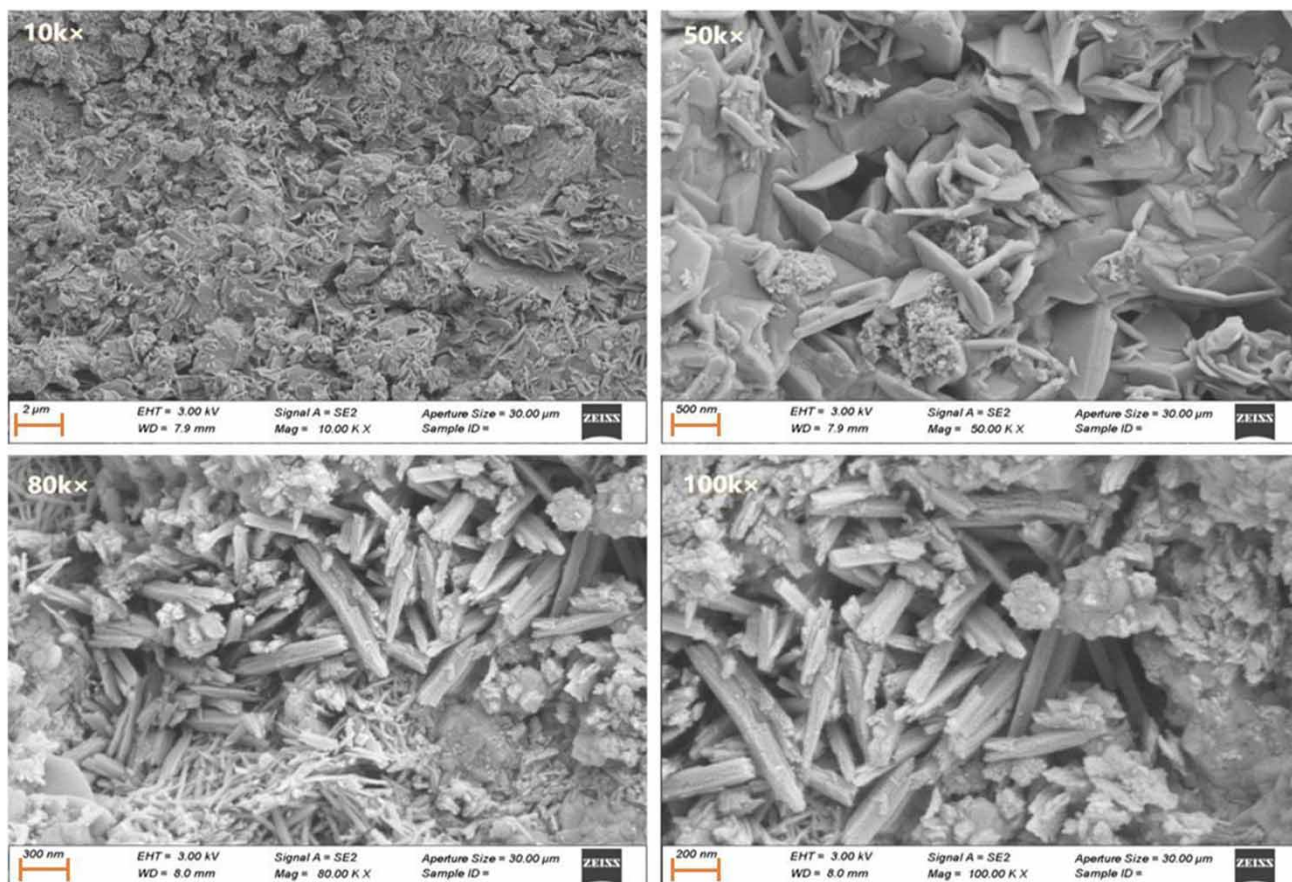
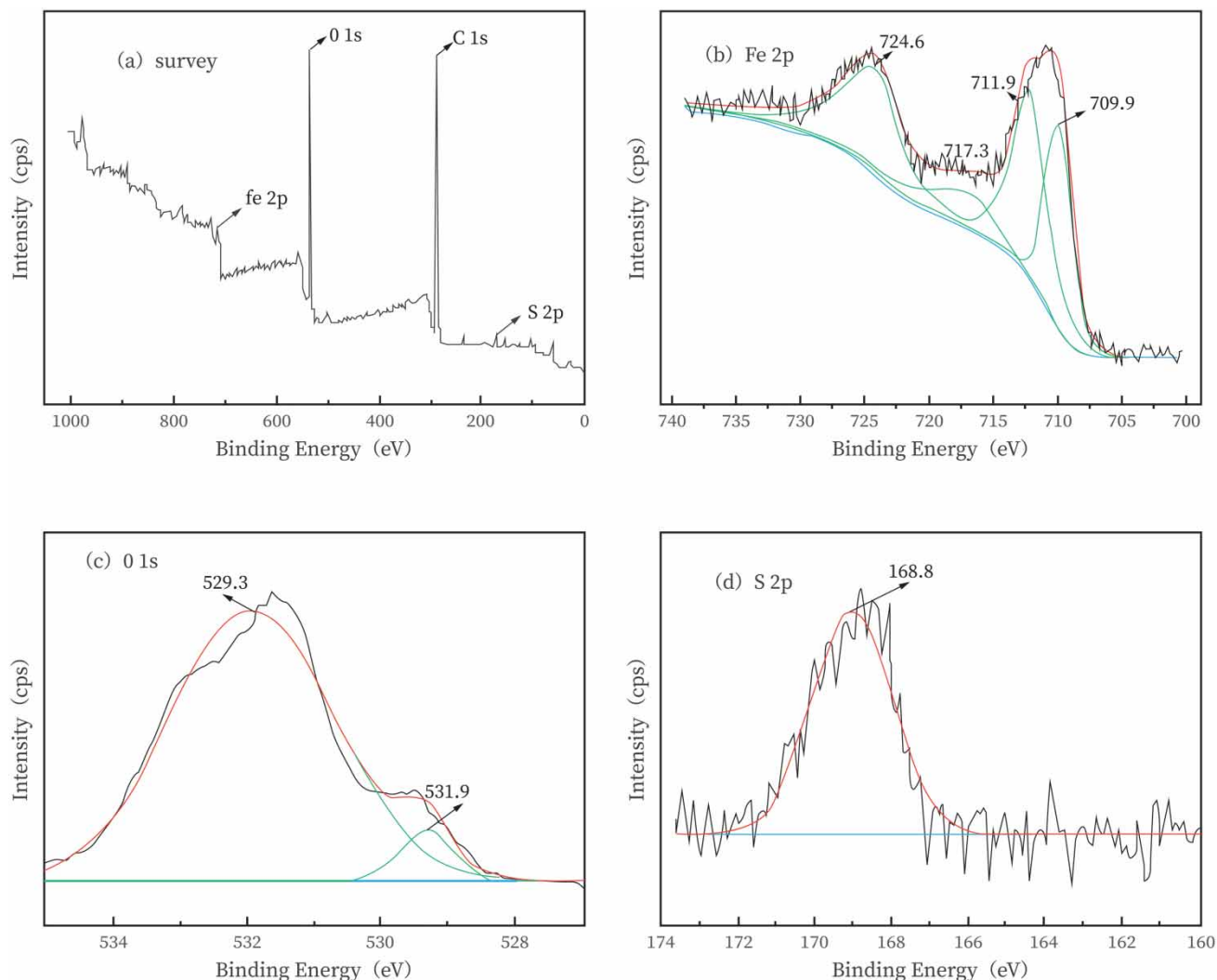


Figure 1 | SEM image of S-Fe (10k  $\times$ , 50k  $\times$ , 80k  $\times$ , 100k  $\times$ ).



**Figure 2** | XPS spectrum of the S-Fe catalyst (a) survey spectrum; (b) Fe2p; (c) O1s; and (d) S2p.

Furthermore, the S2p peak at 168.8 eV indicates that the prepared catalyst contains sulfur, which may exist as sulfate and metal sulfide, as also confirmed by the characterization results of XRD (Figure 2(d)).

### 3.2. Degradation of TCH in different reaction systems

The degradation of TCH (20 mg/L) in five different systems was investigated, as shown in Figure 3. Notably, the degradation rate of TCH was found to be slow when single zero valent iron or catalyst S-Fe was present, indicating poor catalytic efficiency of single catalyst. In case of catalyst S-Fe alone, 10.4% elimination of TCH within 30 min could be attributed to the adsorption by catalyst S-Fe. Moreover, the degradation rate of TCH by non-activated PDS within 30 min was 21.0%, likely due to the presence of some free radicals in PDS that can degrade organic matters despite not being activated. The addition of zero valent iron or S-Fe as activators in presence of PDS significantly boosted the removal rate of TCH. The removal efficiency of TCH in the Fe/PDS system within 30 min was about 75%, showing limited reactivity toward PDS activation. Compared with the Fe/PDS system, the removal efficiency of TCH in the S-Fe/PDS system was higher, reaching 92.6% within 30 min. The decrease of TCH within the first 30 min followed the pseudo-first-order kinetics with a rate constant of  $0.1576 \text{ min}^{-1}$  and correlation coefficient value ( $R^2$ ) of 0.932. These findings indicate that activation of PDS can significantly enhance the removal of TCH, and the catalytic activity can be improved by modifying the iron-based material with sulfur. Based on prior research, it has been suggested that the improvement of catalyst reactivity through sulfur modification could potentially be explained by a hastened rate of electron transfer between PDS and iron species. As suggested

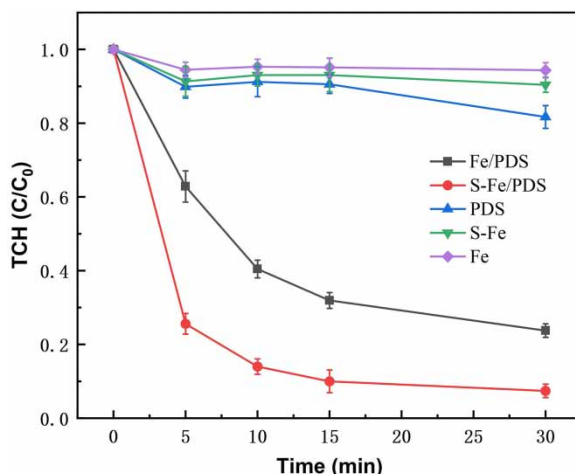


**Figure 3** | Removal efficiencies of TCH in five different systems.

by prior research, the improvement of catalyst reactivity through sulfur modification could be explained by the accelerated electron transfer between PDS and iron species (Wang *et al.* 2020).

### 3.3. Influence of different factors on the catalytic activity of S-Fe

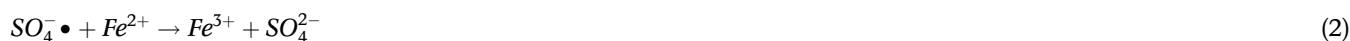
This study aimed to investigate the impact of various factors, including initial TCH concentration, catalyst S-Fe dosage, PDS concentration, solution pH, and coexistence of inorganic anions, on the removal of TCH.

#### 3.3.1. Initial TCH concentration

The degradation of TCH using the S-Fe/PDS system at different initial TCH concentrations is presented in Figure 4(a). Specifically, the highest removal rate of TCH over 30 min was observed at an initial TCH concentration of 20 mg/L (92.6%). As the initial concentration of TCH increased, there was an associated decline in the TCH degradation rate within the system. This trend might be attributed to the adsorption between TCH and the activator S-Fe. With an increasing TCH concentration, a greater amount of TCH molecules were adsorbed onto the S-Fe activator's surface, thereby reducing the available surface area of the activator and suppressing the activation. Consequently, the production of sulfate radical  $SO_4^- \bullet$  in the system was diminished, leading to a reduction in the degradation rate of TCH (Du *et al.* 2016).

#### 3.3.2. Catalyst S-Fe dosage

The impact of the dosage of S-Fe catalyst on TCH degradation is illustrated in Figure 4(b). It was observed that the efficiency of TCH removal gradually increased with an increase in the dosage of the S-Fe catalyst. The highest removal efficiency of TCH was achieved at a dosage of 1.0 g/L. However, at dosages of 2.0 and 3.0 g/L, the efficiency of TCH removal began to decrease. These findings are consistent with findings reported previously (Li & Liu 2022), which suggest that excessive catalyst dosage inhibits the efficacy of the S-Fe/PDS system. This phenomenon implies that  $Fe^{2+}$  in the S-Fe/PDS system consumes  $SO_4^- \bullet$  radicals, as represented in Equations (1) and (2), resulting in the loading of excess  $Fe^{2+}$  at radical sites, which hinders the oxidative decomposition of TCH.



#### 3.3.3. PDS dosage

The impact of PDS concentration on the removal of TCH was found to be significant. The results, as depicted in Figure 4(c), indicate that the degradation rate of TCH increased from 63.4 to 92.6% as the PDS concentration was increased from 0.5 to

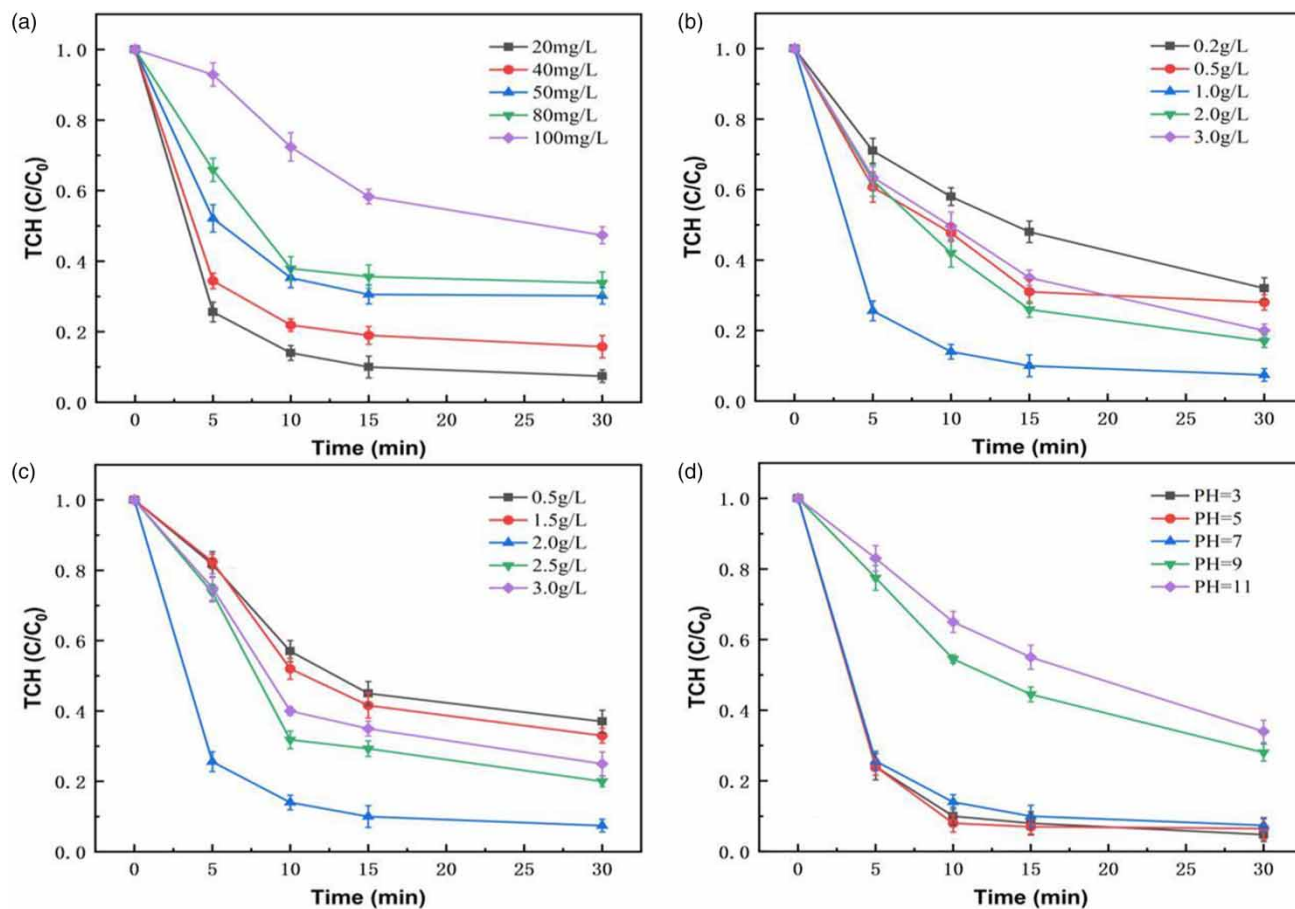


**Figure 4** | Influence factors on the TCH removal efficiency in the S-Fe/PS system (a) TCH concentration ([S-Fe] = 1 g/L, [PDS] = 2 g/L, initial pH = 7); (b) catalyst dosage ([TCH] = 20 mg/L, [PDS] = 2 g/L, initial pH = 7); (c) PDS dosage ([TCH] = 20 mg/L, [S-Fe] = 1 g/L, initial pH = 7); (d) initial pH ([TCH] = 20 mg/L, [PDS] = 2 g/L, [S-Fe] = 1 g/L).

2.0 g/L. However, further increase in PDS dosage to 2.5 and 3.0 g/L led to lower removal rates. This finding is consistent with a previous study by Gayathri *et al.* (2010), which reported that high concentration PDS reduced the decolorization efficiency of the sewage. Two probable reasons may be attributed to this phenomenon. On the one hand, the catalyst surface could offer only a limited number of active sites for PDS activation so that increasing PDS concentration would not promote the degradation of TCH (Park *et al.* 2019). On the other hand, an excess of PDS might lead to radical scavenging, as shown in Equation (3). Specifically, it is suggested that excessive PDS could quench sulfate radicals, thereby leading to reduced removal rates.



### 3.3.4. Initial pH

The impact of different pH values (3, 5, 7, 9, and 11) on the degradation of TCH by the S-Fe/PDS system is presented in Figure 4(d). The results indicated a higher degree of removal efficiency under acidic and neutral conditions (pH of 3, 5, and 7), as opposed to alkaline conditions (pH of 9 and 11). A maximum removal efficiency of 95.1% was observed at pH 3, while removal efficiency decreased as pH increased. This can be attributed to several factors. Firstly, electronic exchange between  $\text{Fe}^{2+}$  and  $\text{Fe}^{3+}$  augments the active site of the activator and Equation (4) only occurs in an acidic reaction system. Secondly, under alkaline conditions,  $\text{SO}_4^{\cdot -}$  is easily converted to  $\cdot\text{OH}$  as shown in Equation (4). Additionally, a multitude of

$\text{OH}^-$  reacts with  $\text{Fe}^{2+}$  or  $\text{Fe}^{3+}$  in an alkaline environment, as shown in Equations (6) and (7).



### 3.3.5. Anions

The impacts of various representative anions, such as chloride ions ( $\text{Cl}^-$ ), sulfate ions ( $\text{SO}_4^{2-}$ ), carbonate ions ( $\text{CO}_3^{2-}$ ), and nitrate ions ( $\text{NO}_3^-$ ), on TCH removal were investigated and are presented in Figure 5. Specifically, Figure 5(a) illustrates that the degradation rate of TCH exhibited a gradual decline as the  $\text{Cl}^-$  concentration increased. This indicates that  $\text{Cl}^-$  has an inhibitory effect on the degradation of TCH in the S-Fe/PDS system. It is suggested that  $\text{Cl}^-$  can be transformed into  $\text{Cl}\cdot$  in the presence of  $\text{SO}_4^{\cdot-}$ , as described in Equation (8) (Anipsitakis *et al.* 2006). Moreover,  $\text{Cl}\cdot$  can react with  $\text{Cl}^-$  to generate dichloro radical ( $\text{Cl}_2^{\cdot-}$ ), as shown in Equation (9) (Huie & Clifton 1990). Therefore, the presence of  $\text{Cl}^-$  is believed to hinder the degradation of TCH in the S-Fe/PDS system.



The impact of  $\text{SO}_4^{2-}$  on TCH degradation is depicted in Figure 5(b). According to the findings of earlier investigations (Wu *et al.* 2015),  $\text{SO}_4^{2-}$  can suppress the redox potential of  $\text{SO}_4^{\cdot-}/\text{SO}_4^{2-}$  within the system, ultimately impeding the activation efficiency of PDS and reducing the rate of TCH removal.

The influence of  $\text{CO}_3^{2-}$  on TCH degradation is illustrated in Figure 5(c). The presence of  $\text{Na}_2\text{CO}_3$  was found to cause a reduction in TCH removal rates by the reaction system. This observation is consistent with findings from previous literature (Yang *et al.* 2019), which reported that  $\text{CO}_3^{2-}$  and  $\text{HCO}_3^-$  have remarkable scavenging effects on  $\text{SO}_4^{\cdot-}$  and  $\cdot\text{OH}$ , as indicated

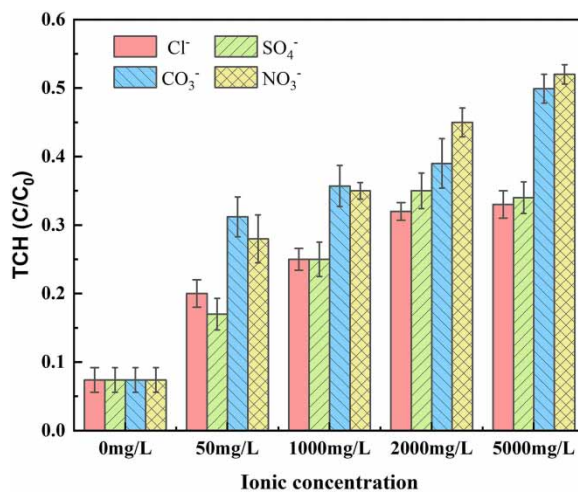


**Figure 5** | Effect of anions on the degradation of TCH by S-Fe activated PDS (a)  $\text{Cl}^-$ ; (b)  $\text{SO}_4^{2-}$ ; (c)  $\text{CO}_3^{2-}$ ; (d)  $\text{NO}_3^-$ . ([TCH] = 20 mg/L, [PDS] = 2 g/L, [S-Fe] = 1 g/L, initial pH = 7, reaction time: 30 min).



in Equations (10)–(13). These reactions lead to a decrease in the reaction rate of TCH in the system.



As shown in Figure 5(d), it was observed that as the concentration of  $NaNO_3$  increased from 0 to 5,000 mg/L, the removal rate of TCH decreased from 92.6 to 48.2%. This finding is consistent with previous reports which indicate that  $NO_3^-$  can compete with organic pollutants for free radicals by reacting with  $SO_4^- \bullet$  (Equation (14)). This leads to a reduction in the degradation efficiency of organic pollutants, as reported by Lee *et al.* (2021).



### 3.4. Activation mechanism

PDS activation can generate various active radicals, such as  $SO_4^- \bullet$ ,  $\bullet OH$ , superoxide radical ( $HO_2 \bullet$ ), and superoxide radical ( $O_2^- \bullet$ ). The identification of active free radicals in the reaction system can be achieved via capturing method, as pointed out by Lai *et al.* (2019). MeOH is commonly used to quench both  $\bullet OH$  ( $9.7 \times 10^8 \text{ M}^{-1} \text{ s}^{-1}$ ) and  $SO_4^- \bullet$  ( $1.6 \times 10^7$ – $7.7 \times 10^7 \text{ M}^{-1} \text{ s}^{-1}$ ), while TBA is more effective in reacting with  $\bullet OH$  ( $4.8 \times 10^8$ – $7.6 \times 10^8 \text{ M}^{-1} \text{ s}^{-1}$ ) but less efficient in capturing  $SO_4^- \bullet$  ( $4.0 \times 10^5$ – $9.1 \times 10^5 \text{ M}^{-1} \text{ s}^{-1}$ ), as reported by He *et al.* (2019).

The present investigation revealed that the introduction of MeOH and TBA, individually, led to a decrease in the degradation rate from 92.6%, to 52.0% and 79.6%, respectively (Figure 6). It can be inferred that both  $SO_4^- \bullet$  and  $\bullet OH$  radicals play a crucial role in the degradation of TCH in the S-Fe/PDS system. Additionally, it was observed that MeOH inhibited the degradation process to a greater extent than TBA. This finding suggests that  $SO_4^- \bullet$  plays a more dominant role in TCH removal than  $\bullet OH$ .

### 3.5. TCH degradation pathway

The intermediate degradation products of TCH were analyzed by liquid chromatography–mass spectrometry (LC–MS). Four intermediate products were observed and the degradation products corresponding to the mass spectrum were determined as  $C_{22}H_{24}N_2O_8$  ( $m/z = 445$ ),  $C_{21}H_{22}N_2O_7$  ( $m/z = 415$ ),  $C_{17}H_{16}O_5$  ( $m/z = 301$ ), and  $C_{15}H_{16}O_5$  ( $m/z = 277$ ).

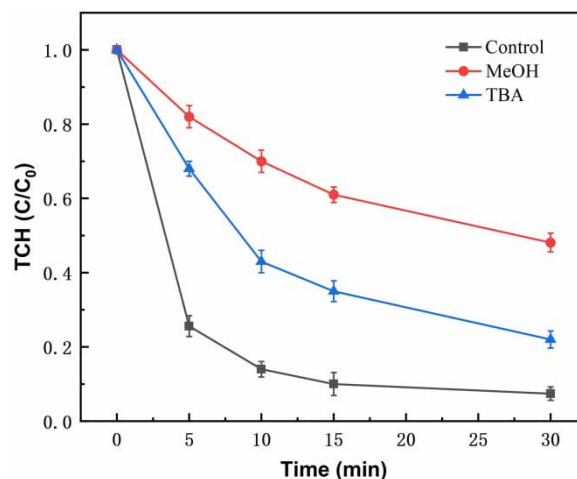


Figure 6 | Degradation of TCH in the S-Fe/PDS system in the presence of different quenchers.

TCH degradation pathway is shown in Supplementary Figure S2. Initially, TCH underwent hydrolysis, resulting in the formation of the molecular ion ( $m/z = 445$ ) (Liang *et al.* 2016). Subsequently, due to the low energy of the C–N bond, the molecule lost a methyl group (Kemou *et al.* 2018) and a hydroxyl group, ultimately forming a substance with a mass of  $m/z = 415$ . Furthermore, free radicals attacked the electron-rich conjugated double bond in the substance with a mass of  $m/z = 415$ , resulting in the generation of the next substance ( $m/z = 301$ ). Lastly, ring opening cracking of the material ion occurred, yielding the final product with a mass of  $m/z = 277$ . Considering the mineralization effect of the S–Fe catalyst on TCH, it is plausible that the products can undergo further decomposition into smaller molecules, ultimately being mineralized into CO<sub>2</sub> and H<sub>2</sub>O.

### 3.6. Reusability of S–Fe

To evaluate the practicability of the catalyst S–Fe, circulation and stability studies were performed. The results indicated that most of the S–Fe catalyst could be adsorbed on a magnet, indicating its magnetism and feasibility for recycling. The degradation rate of TCH within 30 min exhibited a decrease from 92.1% in the first recycling to 91.4% in the second recycling and further decreased to 72.2% in the third recycling, thereby confirming the catalyst's good reusability and stability for organic pollutant removal. The decrease in the degradation rate during the third cycle may be attributed to the loss of catalyst during the cleaning process, continuous precipitation of metal ions in the reaction leading to a decrease in the catalyst activity (Zheng *et al.* 2019). Additionally, a small amount of TCH might have adsorbed onto the surface of the S–Fe catalyst, which could have decreased the surface area of the catalyst and the number of reaction active sites, leading to a subsequent reduction in catalyst activity (Du *et al.* 2016).

## 4. CONCLUSIONS

The preparation of a sulfur-modified iron-based catalyst (S–Fe) was carried out by co-precipitation of sodium thiosulfate and ferrous sulfate in a 1:2 molar ratio. The TCH removal efficiency of the S–Fe/PDS system was found to be higher than that of the Fe/PDS system, with a removal efficiency of approximately 92.6% within 30 min under appropriate conditions, indicating that the catalytic activity could be enhanced by sulfur modification of the iron-based material. Moreover, the S–Fe catalyst exhibited high reusability and stability for removing organic pollutants from wastewater, highlighting the potential application of sulfur-modified iron-based materials as persulfate activators in wastewater treatment.

## ACKNOWLEDGEMENTS

This work was supported by the National Natural Science Foundation of China [grant number 42077323]. The authors also want to thank Dr. Peter Edwards from Purdue University for language editing for this paper.

## CREDIT AUTHOR STATEMENT

S.G.: Data curation, software, writing – original draft preparation, visualization. N.Z.: investigation methodology, validation. L.C.: Conceptualization, writing – reviewing and editing, supervision.

## DATA AVAILABILITY STATEMENT

All relevant data are included in the paper or its Supplementary Information.

## CONFLICT OF INTEREST

The authors declare there is no conflict.

## REFERENCES

- Abejon, R., De Cazes, M., Belleville, M. & Sanchez-Marcano, J. 2015 Large-scale enzymatic membrane reactors for tetracycline degradation in WWTP effluents. *Water Research* **73**, 118–131.
- Acosta, R., Fierro, V., De Yuso, A. M., Nabarlantz, D. & Celzard, A. 2016 Tetracycline adsorption onto activated carbons produced by KOH activation of tyre pyrolysis char. *Chemosphere* **149**, 168–176.

- Anipsitakis, G. P., Dionysiou, D. D. & Gonzalez, M. A. 2006 Cobalt-mediated activation of peroxymonosulfate and sulfate radical attack on phenolic compounds. implications of chloride ions. *Environmental Science & Technology* **40** (3), 1000–1007.
- Borisova, D. A., Vedenyapina, M. D., Krylova, I. V., Rakishev, A. K., Weichgrebe, D., Stopp, P., Rosenwinkel, K. H. & Vedenyapin, A. A. 2013 Electrochemical oxidation of tetracycline on a boron doped diamond electrode within the stability potentials of water. *Russian Chemical Bulletin* **62**, 2590–2594.
- Du, J., Bao, J., Fu, X., Lu, C. & Kim, S. H. 2016 Facile preparation of S/Fe composites as an effective peroxydisulfate activator for RhB degradation. *Separation and Purification Technology* **163**, 145–152.
- Forouzes, M., Ebadi, A. & Aghaeinejad-Meybodi, A. 2019 Degradation of metronidazole antibiotic in aqueous medium using activated carbon as a persulfate activator. *Separation and Purification Technology* **210**, 145–151.
- Gayathri, P., Dorathi, R. P. J. & Palanivelu, K. 2010 Sonochemical degradation of textile dyes in aqueous solution using sulphate radicals activated by immobilized cobalt ions. *Ultrasonics Sonochemistry* **17** (3), 566–571.
- He, J., Xiao, Y., Tang, J., Chen, H. & Sun, H. 2019 Persulfate activation with sawdust biochar in aqueous solution by enhanced electron donor-transfer effect. *Science of The Total Environment* **690**, 768–777.
- Huie, R. E. & Clifton, C. L. 1990 Temperature dependence of the rate constants for reactions of the sulfate radical,  $\text{SO}_4^-$ , with anions. *Journal of Physical Chemistry* **94** (23), 8561–8567.
- Iakovides, I. C., Michael-Kordatou, I., Moreira, N. F. F., Ribeiro, A. R., Fernandes, T., Pereira, M. F. R., Nunes, O. C., Manaia, C. M., Silva, A. M. T. & Fatta-Kassinos, D. 2019 Continuous ozonation of urban wastewater: removal of antibiotics, antibiotic-resistant *Escherichia coli* and antibiotic resistance genes and phytotoxicity. *Water Research* **159**, 333–347.
- Kemmou, L., Frontistis, Z., Vakros, J., Manariotis, I. D. & Mantzavinos, D. 2018 Degradation of antibiotic sulfamethoxazole by biochar-activated persulfate: factors affecting the activation and degradation processes. *Catalysis Today* **313**, 128–133.
- Kovalakova, P., Cizmas, L., McDonald, T. J., Marsalek, B., Feng, M. & Sharma, V. K. 2020 Occurrence and toxicity of antibiotics in the aquatic environment: a review. *Chemosphere* **251**, 126351.
- Lai, C., Huang, F., Zeng, G., Huang, D., Qin, L., Cheng, M., Zhang, C., Li, B., Yi, H., Liu, S., Li, L. & Chen, L. 2019 Fabrication of novel magnetic  $\text{MnFe}_2\text{O}_4$ /bio-char composite and heterogeneous photo-Fenton degradation of tetracycline in near neutral pH. *Chemosphere* **224**, 910–921.
- Lee, D., Kim, S., Tang, K., De Volder, M. & Hwang, Y. 2021 Oxidative degradation of tetracycline by magnetite and persulfate: performance, water matrix effect, and reaction mechanism. *Nanomaterials* **11** (9), 2292.
- Li, H. & Liu, N. 2022 Application of FeS-activated persulfate oxidation system for the degradation of tetracycline in aqueous solution. *Environmental Science and Pollution Research* **30** (4), 10745–10755.
- Li, S. Z., Li, X. Y. & Wang, D. Z. 2004 Membrane (RO-UF) filtration for antibiotic wastewater treatment and recovery of antibiotics. *Separation and Purification Technology* **34** (1–3), 109–114.
- Liang, Z., Cao, Y., Li, Y., Xie, J., Guo, N. & Jia, D. 2016 Solid-state chemical synthesis of rod-like fluorine-doped  $\beta\text{-Bi}_2\text{O}_3$  and their enhanced photocatalytic property under visible light. *Applied Surface Science* **390**, 78–85.
- Ling, C., Wu, S., Dong, T., Dong, H., Wang, Z., Pan, Y. & Han, J. 2022 Sulfadiazine removal by peroxymonosulfate activation with sulfide-modified microscale zero-valent iron: major radicals, the role of sulfur species, and particle size effect. *Journal of Hazardous Materials* **423**, 127082.
- Ma, J., Song, W., Chen, C., Ma, W., Zhao, J. & Tang, Y. 2005 Fenton degradation of organic compounds promoted by dyes under visible irradiation. *Environmental Science & Technology* **39** (15), 5810–5815.
- Nasseri, S., Mahvi, A. H., Seyedsalehi, M., Yaghmaeian, K., Nabizadeh, R., Alimohammadi, M. & Safari, G. H. 2017 Degradation kinetics of tetracycline in aqueous solutions using peroxydisulfate activated by ultrasound irradiation: effect of radical scavenger and water matrix. *Journal of Molecular Liquids* **241**, 704–714.
- Park, J. H., Wang, J. J., Tafti, N. & Delaune, R. D. 2019 Removal of Eriochrome Black T by sulfate radical generated from Fe-impregnated biochar/persulfate in Fenton-like reaction. *Journal of Industrial and Engineering Chemistry* **71**, 201–209.
- Qi, C., Liu, X., Ma, J., Lin, C., Li, X. & Zhang, H. 2016 Activation of peroxymonosulfate by base: implications for the degradation of organic pollutants. *Chemosphere* **151**, 280–288.
- Saadati, F., Keramati, N. & Ghazi, M. M. 2016 Influence of parameters on the photocatalytic degradation of tetracycline in wastewater: a review. *Critical Reviews in Environmental Science and Technology* **46**, 757–782.
- Shen, Q., Wang, Z., Yu, Q., Cheng, Y., Liu, Z., Zhang, T. & Zhou, S. 2020 Removal of tetracycline from an aqueous solution using manganese dioxide modified biochar derived from Chinese herbal medicine residues. *Environmental Research* **183**, 109195.
- Waclawek, S., Lutze, H. V., Grübel, K., Padil, V. V., Černík, M. & Dionysiou, D. D. 2017 Chemistry of persulfates in water and wastewater treatment: a review. *Chemical Engineering Journal* **330**, 44–62.
- Wang, H., Chen, T., Chen, D., Zou, X., Li, M., Huang, F., Sun, F., Wang, C., Shu, D. & Liu, H. 2020 Sulfurized oolitic hematite as a heterogeneous Fenton-like catalyst for tetracycline antibiotic degradation. *Applied Catalysis B-Environmental* **260**, 118203.
- Weidner, E., Siwińska-Ciesielczyk, K., Moszyński, D., Jesionowski, T. & Ciesielczyk, F. 2021 A comprehensive method for tetracycline removal using lanthanum-enriched titania-zirconia oxide system with tailored physicochemical properties. *Environmental Technology & Innovation* **24**, 102016.
- Wu, X., Gu, X., Lu, S., Qiu, Z., Sui, Q., Zang, X., Miao, Z. & Xu, M. 2015 Strong enhancement of trichloroethylene degradation in ferrous ion activated persulfate system by promoting ferric and ferrous ion cycles with hydroxylamine. *Separation and Purification Technology* **147**, 186–193.

- Yang, L., Xue, J., He, L., Wu, L., Ma, Y., Chen, H., Li, H., Peng, P. & Zhang, Z. 2019 Review on ultrasound assisted persulfate degradation of organic contaminants in wastewater: influences, mechanisms and prospective. *Chemical Engineering Journal* **378**, 122146.
- Zhang, M., Chen, X., Zhou, H., Muruganathan, M. & Zhang, Y. 2015 Degradation of p-nitrophenol by heat and metal ions co-activated persulfate. *Chemical Engineering Journal* **264**, 39–47.
- Zhang, Y., Liu, H., Xin, Y., Shen, Y., Wang, J., Cai, C. & Wang, M. 2019 Erythromycin degradation and ERY-resistant gene inactivation in erythromycin mycelial dreg by heat-activated persulfate oxidation. *Chemical Engineering Journal* **358**, 1446–1453.
- Zheng, H., Bao, J., Huang, Y., Xiang, L., Faheem, Ren, B., Du, J., Nadagouda, M. N. & Dionysiou, D. D. 2019 Efficient degradation of atrazine with porous sulfurized Fe<sub>2</sub>O<sub>3</sub> as catalyst for peroxymonosulfate activation. *Applied Catalysis B-Environmental* **259**, 118056.

First received 21 March 2023; accepted in revised form 19 May 2023. Available online 2 June 2023